3rd International Conference on Material and Component Performance
under Variable Amplitude Loading, VAL2015

# Invariant-Based and Critical-Plane Rainflow Approaches for Fatigue Life Prediction under Multiaxial Variable Amplitude Loading

Marco Antonio Meggiolaro[a], Jaime Tupiassú Pinho de Castro[a,*], Hao Wu[b]

*[a]Dept. of Mechanical Engineering, Pontifical Catholic University of Rio de Janeiro, Brazil*
*[b]School of Aerospace Engineering and Applied Mechanics, Tongji University, Shanghai, P.R. China*

**Abstract**

Multiaxial variable amplitude histories usually require a rainflow algorithm to identify individual cycles. A computationally-efficient 5D multiaxial rainflow algorithm that can deal with any 1D to 6D history has been proposed by the authors, based on the representation of 6D stresses and strains in 5D deviatoric sub-spaces that use a von Mises metric. These spaces provide simple geometric interpretations for the identified load cycles while highly reducing computational cost. In this work, the most efficient multiaxial rainflow algorithms for variable amplitude histories are presented and compared, detailing their individual advantages and disadvantages.

## 1. Introduction

   The identification of individual cycles of variable amplitude loading (VAL) histories is required for applying most fatigue damage models, but the traditional rainflow algorithm cannot be directly applied to multiaxial histories, since it can count only one stress or strain component. A possible approach to solve this problem is to project the multiaxial stress or strain VAL history onto a so-called candidate plane, where the crack is assumed to initiate at the critical point

   * Corresponding author. Tel.: +55-21-35271642.
     *E-mail address:* jtcastro@puc-rio.br

of the structural component. The number of such planes can be narrowed down to a manageable size assuming that the fatigue failure mechanism is associated with a single dominant crack [1], as usual in most metallic alloys, and free surface conditions, i.e. $\tau_{xz} = \tau_{yz} = 0$ and $\gamma_{xz} = \gamma_{yz} = 0$, where **z** is perpendicular to the surface. The free-surface formulation can allow the presence of a compressive surface stress $\sigma_z = -p \leq 0$ caused by a surface pressure $p \geq 0$. Under these conditions, the stresses and strains projected onto a candidate plane rotated at $(\theta, \phi)$ from the surface, as illustrated in Fig. 1, become

$$\tau_A(\theta, \phi) = (\tau_{xy}\cos 2\theta + 0.5 \cdot (\sigma_y - \sigma_x) \cdot \sin 2\theta) \cdot \sin\phi$$
$$\tau_B(\theta, \phi) = 0.5 \cdot (\sigma_x \cdot \cos^2\theta + \sigma_y \cdot \sin^2\theta + p + \tau_{xy}\sin 2\theta) \cdot \sin 2\phi$$
$$\sigma_\perp(\theta, \phi) = (\sigma_x \cdot \cos^2\theta + \sigma_y \cdot \sin^2\theta + \tau_{xy}\sin 2\theta) \cdot \sin^2\phi - p \cdot \cos^2\phi$$
$$\gamma_A(\theta, \phi) = (\gamma_{xy}\cos 2\theta + (\varepsilon_y - \varepsilon_x) \cdot \sin 2\theta) \cdot \sin\phi \tag{1}$$
$$\gamma_B(\theta, \phi) = (\varepsilon_x \cdot \cos^2\theta + \varepsilon_y \cdot \sin^2\theta - \varepsilon_z + 0.5 \cdot \gamma_{xy}\sin 2\theta) \cdot \sin 2\phi$$
$$\varepsilon_\perp(\theta, \phi) = (\varepsilon_x \cdot \cos^2\theta + \varepsilon_y \cdot \sin^2\theta + 0.5 \cdot \gamma_{xy}\sin 2\theta) \cdot \sin^2\phi + \varepsilon_z \cdot \cos^2\phi$$

where $\sigma_\perp$ and $\varepsilon_\perp$ are the normal stress and strain perpendicular to the candidate plane, $\tau_A$ and $\gamma_A$ are the shear stress and strain parallel to the free surface, and $\tau_B$ and $\gamma_B$ are the shear stress and strain in the depth direction, see Fig. 1, while $\sigma_x$, $\sigma_y$, $\tau_{xy}$, $\varepsilon_x$, $\varepsilon_y$ and $\gamma_{xy}$ are the time-varying stress and strain components caused by the VAL history. Under such free-surface conditions, the expected fatigue cracks can be classified into three types: Case A tensile, Case A shear, and Case B shear cracks, explained as follows.
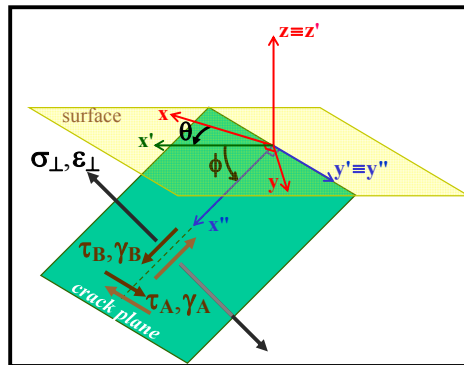


Fig. 1: Stress and strain components acting on a candidate plane $(\theta, \phi)$ under free surface conditions, possibly with a surface pressure $p = -\sigma_z \geq 0$.

If the surface is unpressurized ($p = 0$), then for any given $\theta$ and any loading history it follows from Eq. (1) that both the ranges and the magnitudes of $\sigma_\perp$, $\tau_A$, $\varepsilon_\perp$ and $\gamma_A$ are maximized for planes which obey $\sin^2\phi = \sin\phi = 1$, i.e. for candidate planes $(\theta, 90^o)$ perpendicular to the free surface. This conclusion is valid even for non-proportional (NP) VAL histories, since the factors $\sin^2\phi$ or $\sin\phi$ multiply these stresses and strains for every single cycle. Fatigue cracks that initiate in planes with $\phi = 90^o$ are called Case A cracks, which can be driven either in Mode I if $\sigma_\perp$ and $\varepsilon_\perp$ dominate, or in Mode II if $\tau_A$ and $\gamma_A$ dominate the damage process, generating respectively the Case A tensile and Case A shear cracks.

If a surface pressure $p > 0$ is applied, Case A cracks would not be affected because the magnitude of the normal stress perpendicular to their planes $\sigma_\perp(\theta, \phi)$ would still be maximized for $\phi = 90^o$, hence in such cases all terms involving $p$ would vanish in the above equations. Note that large pressure variations $\Delta p$, due e.g. to Hertzian contact fatigue, could maximize the normal strain range $\Delta \varepsilon_\perp(\theta, \phi)$ for $\phi = 0^o$, however a $\phi = 0^o$ critical plane parallel to the free surface would be unlikely since the associated normal stress $\sigma_\perp(\theta, 0^o) = -p$ would always be compressive, so it would inhibit the crack propagation process.

On the other hand, Eq. (1) shows that the ranges and magnitudes of $\tau_B$ and $\gamma_B$ are maximized for planes with $\sin 2\phi = 1$, i.e. in candidate planes making $45^o$ with the free surface. The cracks that initiate in such $\phi = 45^o$ inclined planes are called Case B cracks, which are always driven in Mode III (due to the maximization of the $\tau_B$ and $\gamma_B$ ranges and

magnitudes) with the possibility of a Mixed II-III behaviour (if $\tau_A$ and $\gamma_A$ in such $\phi = 45^o$ plane are also significant when compared to $\tau_B$ and $\gamma_B$).

For each candidate plane projection, a special critical plane rainflow algorithm can be used to identify individual half-cycles and the corresponding fatigue damage caused by the VAL. For Case A cracks, a uniaxial rainflow count is enough, if it is applied to the main stress or strain component responsible for fatigue damage, such as the normal stress (or strain) for Case A tensile and the shear stress (or strain) for Case A shear cracks. For Mode III Case B cracks, a uniaxial rainflow is enough if applied to the Mode III shear stress (or strain) component. However, mixed Mode II-III Case B cracks suffer the combined influence of two shear components (responsible for Modes II and III), which requires a bi-dimensional rainflow count, explained in the next sections.

Several candidate planes must be studied to find the critical plane where the crack should initiate. This process requires, for each candidate plane, a critical-plane rainflow count procedure followed by the determination of equivalent stress or strain ranges associated with each counted half-cycle, which are then used to calculate the associated fatigue damage. The critical plane where the crack should initiate is then the candidate plane with the highest accumulated fatigue damage.

Another approach is to use a truly multiaxial rainflow algorithm such as the one proposed by Wang and Brown [2], or its improved version from [3], which identify individual half-cycles within multiaxial NP histories simultaneously considering all six stress or strain components, based on a Mises metric. No stress or strain projections are necessary, as opposed to the critical plane approach. So this method is more straightforward, since it requires a single rainflow counting procedure for each multiaxial VAL history, as opposed to the critical plane approach, where each projection of the VAL history onto a candidate plane is individually rainflow counted.

Both multiaxial rainflow approaches use as inputs both stress and strain paths, which for elastoplastic VAL histories can be correlated from proper incremental plasticity calculations. The rainflow outputs are multiaxial path segments associated with each individual half-cycle. Depending on the damage model, scalar equivalent strain or stress ranges and mean components must be calculated from such multiaxial segments, which can be performed e.g. using a convex enclosure approach or the moment of inertia (MOI) method [4]. In the next sections, the two most adopted multiaxial approaches for the rainflow counting method are described and compared.

## 2. Wang-Brown Multiaxial Rainflow

Wang and Brown [2] proposed a multiaxial generalization of the rainflow count that is applicable to any proportional or NP strain history. It can also be applied to stresses, with simple modifications to the algorithm. The original Wang-Brown algorithm requires the computation of a relative Mises strain range $\Delta\varepsilon_{Mises}$ between each loading state and all remaining loading states in the history. This algorithm focuses on periodic load histories where each period consists of a relatively few number of cycles. Therefore, such formulation is impractical for truly VAL histories, where no simple periodic loading blocks can be identified. In addition, the formulation of the Wang-Brown algorithm in the 6D strain (or stress) space requires the calculation of the intersection between 6D hyper-ellipsoids to identify the rainflow cycles [3].

The Modified Wang-Brown method proposed in [3] solves all such problems, working in the reduced 5D deviatoric stress $\mathbf{E_{5s}}$ or strain $\mathbf{E_{5e}}$ spaces, or in a lower dimension sub-space of them. In this way, a general multiaxial strain history is represented by a set of 5D points

$$\mathbf{P_i} = (e_1, e_2, e_3, e_4, e_5) \equiv 0.5 \cdot \left(2\varepsilon_x - (\varepsilon_y + \varepsilon_z),\ (\varepsilon_y - \varepsilon_z)\sqrt{3},\ \gamma_{xy}\sqrt{3},\ \gamma_{xz}\sqrt{3},\ \gamma_{yz}\sqrt{3}\right) \tag{2}$$

while a multiaxial stress history defines instead the 5D points

$$\mathbf{P_i} = (s_1, s_2, s_3, s_4, s_5) \equiv \left(\sigma_x - (\sigma_y + \sigma_z)/2,\ (s_y - s_z)\sqrt{3}/2,\ \tau_{xy}\sqrt{3},\ \tau_{xz}\sqrt{3},\ \tau_{yz}\sqrt{3}\right) \tag{3}$$

Wang-Brown's multiaxial rainflow algorithm is rather simplified when working in such 5D spaces, because the distance between two points **A** and **B** is already proportional to the relative $\Delta\sigma_{Mises}$ or $\Delta\varepsilon_{Mises}$ between them, since

$$|\vec{s}_B' - \vec{s}_A'| = \Delta\sigma_{Mises} \text{ and } |\vec{e}_B' - \vec{e}_A'| = (1 + \bar{v}) \cdot \Delta\varepsilon_{Mises} \tag{4}$$

When applied to invariant-based equivalent stress or strain multiaxial fatigue damage models, such as the Sines [5] and Crossland [6] models, a measure of an equivalent strain range is required for each half-cycle. The Mises

relative strain range $\Delta\varepsilon_{Mises}$ between the two strain states from each half-cycle cannot be used as such equivalent range, because it would assume that all half-cycles are straight lines without any NP effect. The NP effects can only be accounted for if the path shape between any two counted strain states is considered, e.g. using the MOI method or other equivalent range approaches from [4]. Wang-Brown's original multiaxial rainflow rules have been improved in [3], generating the so-called modified Wang-Brown (MWB) counting.

This 5D algorithm implementation is applicable to invariant-based equivalent stress or strain models, such as the Sines [5] or Crossland [6] models, or to any other fatigue damage model that allows the mixture of stress or strain components happening on different planes. Note however that such 5D-counted half-cycles should not be applied to a critical plane approach, because the original history was not projected onto candidate planes before the rainflow.

If, on the other hand, a critical plane approach is used, the MWB rainflow algorithm must be applied exclusively to the 2D shear path in the $\tau_B \times \tau_A$ or $\gamma_B \times \gamma_A$ diagram, to find the rainflow-counted equivalent shear ranges for the specific search of Case B mixed Mode II-III shear cracks. The MWB algorithm must be applied in this case to every Case B candidate plane to search for the Case B mixed Mode II-III shear crack with maximum damage. Note that the critical plane search for Case A Mode I, Case A Mode II and Case B Mode III cracks does not need the MWB, only a uniaxial rainflow count is required, as discussed in the next sections.

## 3. Critical Plane Approach

The Wang-Brown algorithm performs a multiaxial rainflow count on the original 6D stress or strain history, calculating the path segments associated with each half-cycle. The Modified Wang-Brown results in similar 6D rainflow counts, but performed on a more efficient 5D deviatoric space. However, such half-cycles should not be projected onto candidate planes to be used in a critical plane approach, because each candidate plane could have a very different rainflow count.

So, to deal with VAL histories, the critical plane approach needs to first project the 6D stress or strain history onto each candidate plane, and only after that a rainflow count should be evaluated. The actual procedures are different depending on the tensile or on the shear nature of the crack, as described next.

### 3.1 Case A tensile and shear cracks

The initiation of Case A cracks, which grow along a critical plane perpendicular to the free surface, is controlled by the combination of the four stresses and strains obtained from Eq. (1) for $\phi = 90^o$:

$$\tau_A(\theta, 90^o) = \tau'_{xy}(\theta) = \tau_{xy}\cos 2\theta + 0.5\cdot(\sigma_y - \sigma_x)\cdot\sin 2\theta$$
$$\sigma_\perp(\theta, 90^o) = \sigma'_x(\theta) = \sigma_x\cdot\cos^2\theta + \sigma_y\cdot\sin^2\theta + \tau_{xy}\sin 2\theta$$
$$\gamma_A(\theta, 90^o) = \gamma_{xy}\cos 2\theta + (\varepsilon_y - \varepsilon_x)\cdot\sin 2\theta \tag{5}$$
$$\varepsilon_\perp(\theta, 90^o) = \varepsilon_x\cdot\cos^2\theta + \varepsilon_y\cdot\sin^2\theta + 0.5\cdot\gamma_{xy}\sin 2\theta$$

where $\sigma_x$, $\sigma_y$, $\tau_{xy}$, $\varepsilon_x$, $\varepsilon_y$ and $\gamma_{xy}$ are time-varying components defined by the load history.

Figure 2 shows the stress states and Mohr circles associated with Case A cracks, which reflect the above equations. As discussed before, Case A cracks can be divided into shear or tensile types. The dominant failure mechanism of several materials is Mode II *shear* crack nucleation and growth. Case A *shear* cracks will most likely initiate in these shear-sensitive materials in $\theta$ directions that maximize the ranges of the shear components $\tau_A$ and $\gamma_A$, with the normal components $\sigma_\perp$ and $\varepsilon_\perp$ only playing a secondary role affecting microcrack closure. But other materials, such as 304 stainless steel (under certain load histories) and cast irons, fail predominantly by Mode I microcrack and crack growth on planes of maximum tensile strain or stress. Case A *tensile* cracks will most likely initiate in these tensile-sensitive materials in $\theta$ directions that maximize the ranges, the means and/or the maxima of the Mode I normal components $\sigma_\perp$ and $\varepsilon_\perp$ (with little or no influence of $\tau_A$ and $\gamma_A$).
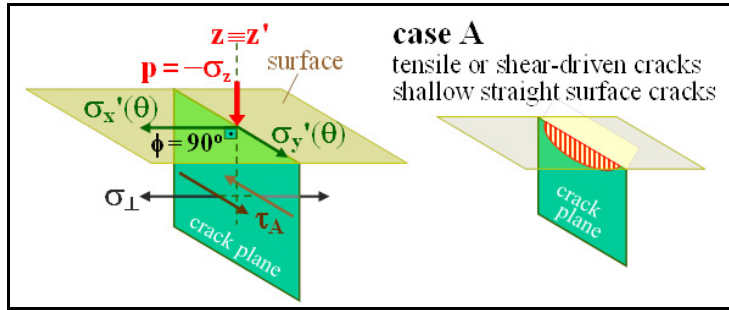
Fig. 2: Stress states and Mohr circles for a Case A crack in a **(θ, 90º)** plane under free surface conditions with a surface pressure **p**.

### *3.2 Case B shear cracks*

The initiation of Case B cracks (with $\phi = 45º$), on the other hand, is always controlled by shear. These cracks are the ones described by the intrusion-extrusion model, where the slip bands are mainly caused by the range of the shear stress $\tau_B(\theta, 45º)$, which induces Mode III out-of-plane tearing at the maximum crack depth. The presence of $\tau_B(\theta, 45º)$ parallel to the crack plane along its depth makes Case B (Mode III) surface microcracks become much deeper than Case A (Mode II) microcracks, which are usually shallow due to $\tau_B(\theta, 90º) = 0$. However, the damage process is not caused solely by the range of $\tau_B$. Combinations of all shear stresses and strains $\tau_A$, $\tau_B$, $\gamma_A$, and $\gamma_B$ parallel to crack plane are the main cause of Case B crack initiation, maybe with some influence of the maximum or mean normal stress $\sigma_\perp$ (and perhaps even $\varepsilon_\perp$) due to the opening and closure of microcracks. The six stress and strain components from a Case B candidate plane $(\theta, 45º)$ are then obtained from replacing $\phi = 45º$ in Eq. (1), giving

$$\tau_A(\theta, 45^o) = (\tau_{xy} \cos 2\theta + 0.5 \cdot (\sigma_y - \sigma_x) \cdot \sin 2\theta)/\sqrt{2}$$
$$\tau_B(\theta, 45^o) = (\sigma_x \cdot \cos^2 \theta + \sigma_y \cdot \sin^2 \theta + p + \tau_{xy} \sin 2\theta)/2 = \sigma_\perp(\theta, 45^o) + p$$
$$\sigma_\perp(\theta, 45^o) = (\sigma_x \cdot \cos^2 \theta + \sigma_y \cdot \sin^2 \theta - p + \tau_{xy} \sin 2\theta)/2 = \tau_B(\theta, 45^o) - p$$
$$\gamma_A(\theta, 45^o) = (\gamma_{xy} \cos 2\theta + (\varepsilon_y - \varepsilon_x) \cdot \sin 2\theta)/\sqrt{2}$$
$$\gamma_B(\theta, 45^o) = \varepsilon_x \cdot \cos^2 \theta + \varepsilon_y \cdot \sin^2 \theta - \varepsilon_z + 0.5 \cdot \gamma_{xy} \sin 2\theta = 2 \cdot (\varepsilon_\perp(\theta, 45^o) - \varepsilon_z)$$
$$\varepsilon_\perp(\theta, 45^o) = (\varepsilon_x \cdot \cos^2 \theta + \varepsilon_y \cdot \sin^2 \theta + 0.5 \cdot \gamma_{xy} \sin 2\theta + \varepsilon_z)/2 = \varepsilon_z + \gamma_B(\theta, 45^o)/2$$

$$(6)$$

Figure 3 shows the stress states and Mohr circles associated with Case B cracks, which reflect these equations.
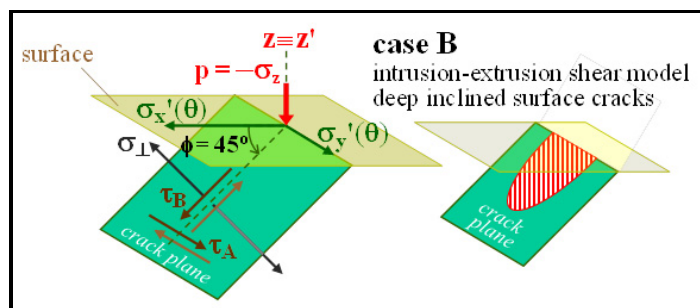


Fig. 3: Stress states and Mohr circles for a Case B crack **(θ, 45º)** for a free surface with surface pressure **p**.

## 4. Critical Plane Rainflow

For Case A cracks, which initiate along a plane perpendicular to a free surface ($\phi = 90º$), a sequential uniaxial rainflow count can be performed on the main stress or strain channel. Shear-based damage models require a uniaxial

rainflow count applied to the shear strain $\gamma_A$ (or stress $\tau_A$) acting on the candidate plane, while tensile-based damage models must count the normal strain $\varepsilon_\perp$ (or stress $\sigma_\perp$) perpendicular to such plane. The other stress and strain components can be regarded as auxiliary channels [7], which will provide the additional parameters needed by each multiaxial fatigue damage model, such as mean or maximum stresses.

For instance, Fatemi-Socie's [8] shear-based model combines $\Delta\gamma_A$ and $\sigma_{\perp max}$ to calculate the accumulated damage for each Case A candidate plane, which is maximized for the critical plane where the crack is expected to initiate. Therefore, the main channel $\gamma_A$ must be rainflow counted using a uniaxial algorithm, while the associated $\sigma_{\perp max}$ (the maximum normal stresses $\sigma_\perp$ along each counted half-cycle) must be identified from the auxiliary channel $\sigma_\perp$. This procedure involving a uniaxial count on a main channel and the tracking of other auxiliary channels is called here the critical plane rainflow algorithm.

On the other hand, Smith-Watson-Topper's (SWT) [9] tensile-based damage model combines $\Delta\varepsilon_\perp$ and $\sigma_{\perp max}$ for each Case A candidate plane, therefore the critical plane rainflow must be applied to the main channel $\varepsilon_\perp$ while the associated $\sigma_{\perp max}$ are obtained from the auxiliary channel $\sigma_\perp$.

As a general rule, damage models used to predict Case A tensile cracks must apply the critical plane rainflow to the main channel $\sigma_\perp$ (Generalized Goodman) or $\varepsilon_\perp$ (SWT [9], Liu-I [10]), while for Case A shear cracks the main channel should be $\tau_A$ (Findley [11], McDiarmid-A [12]) or $\gamma_A$ (Fatemi-Socie [8], Brown-Miller [13], Liu-II [10]). For Case B shear cracks, the main rainflow channel should be $\tau_B$ (Findley [11], McDiarmid-B [12]) or $\gamma_B$ (Fatemi-Socie [8], Brown-Miller [13], Liu-II [10]), with the remaining components acting as auxiliary channels. Table 1 summarizes for each damage model the main channel to be rainflow counted, the auxiliary channels to be tracked, and the resulting identified parameters for each half-cycle. Note that, in addition to the use of either the stress ratio $R = \sigma_{\perp min}/\sigma_{\perp max}$ or the mean $\sigma_{\perp m} = (\sigma_{\perp max} + \sigma_{\perp min})/2$, the main difference among the critical plane implementations of Liu's energy model is that the main rainflow channel is either $\varepsilon_\perp$ for Case A Mode I tensile cracks, $\gamma_A$ for Case A Mode II shear cracks, or $\gamma_B$ for Case B Mode III shear cracks.

Table 1: Main and auxiliary input channels involved in the critical plane rainflow algorithm, along with the identified main output range and remaining output parameters used in each damage model for Case A Mode I tensile ($A_I$), Case A Mode II shear ($A_{II}$) and Case B Mode III ($B_{III}$) shear cracks.

| | Model | Main | Auxiliary | Range | Parameters |
|---|---|---|---|---|---|
| $A_I$ | Generalized Goodman | $\sigma_\perp$ | - | $\Delta\sigma_\perp$ | $\sigma_m = \sigma_{\perp max} - \Delta\sigma_\perp$ |
| | Smith-Watson-Topper | $\varepsilon_\perp$ | $\sigma_\perp$ | $\Delta\varepsilon_\perp$ | $\sigma_{\perp max}$ |
| | Liu-I | $\varepsilon_\perp$ | $\sigma_\perp, \tau_A, \gamma_A$ | $\Delta\varepsilon_\perp$ | $\Delta\sigma_\perp, \Delta\tau_A, \Delta\gamma_A, R$ |
| $A_{II}$ | Findley, McDiarmid-A | $\tau_A$ | $\sigma_\perp$ | $\Delta\tau_A$ | $\sigma_{\perp max}$ |
| | Fatemi-Socie | $\gamma_A$ | $\sigma_\perp$ | $\Delta\gamma_A$ | $\sigma_{\perp max}$ |
| | Brown-Miller | $\gamma_A$ | $\varepsilon_\perp$ | $\Delta\gamma_A$ | $\Delta\varepsilon_\perp$ |
| | Liu-II | $\gamma_A$ | $\sigma_\perp, \varepsilon_\perp, \tau_A$ | $\Delta\gamma_A$ | $\Delta\sigma_\perp, \Delta\varepsilon_\perp, \Delta\tau_A, \sigma_{\perp m}$ |
| $B_{III}$ | Findley, McDiarmid-B | $\tau_B$ | $\sigma_\perp$ | $\Delta\tau_B$ | $\sigma_{\perp max}$ |
| | Fatemi-Socie | $\gamma_B$ | $\sigma_\perp$ | $\Delta\gamma_B$ | $\sigma_{\perp max}$ |
| | Brown-Miller | $\gamma_B$ | $\varepsilon_\perp$ | $\Delta\gamma_B$ | $\Delta\varepsilon_\perp$ |
| | Liu-II | $\gamma_B$ | $\sigma_\perp, \varepsilon_\perp, \tau_B$ | $\Delta\gamma_B$ | $\Delta\sigma_\perp, \Delta\varepsilon_\perp, \Delta\tau_B, \sigma_{\perp m}$ |

A very efficient uniaxial rainflow algorithm that is capable of dealing with auxiliary channels has been proposed in [7]. It is based on the four-point rainflow algorithm [14], which is able to count very long histories in real time as the peaks and valleys are entered as input, without requiring an *a priori* knowledge of the entire load history. In this "critical plane rainflow" algorithm, each stack entry stores not only the main channel to be counted (e.g. $\gamma_A$ for Fatemi-Socie's model), but also the maximum and minimum values of any auxiliary channel required by the chosen multiaxial fatigue damage model (such as the minimum and maximum normal stresses $\sigma_{\perp min}$ and $\sigma_{\perp max}$). Then, every time a half-cycle is counted and eliminated from the stack, the previous stack element inherits the minimum and maximum values of the auxiliary channel (e.g. $\sigma_{\perp min}$ and $\sigma_{\perp max}$) among itself and the eliminated elements, automatically keeping track of their variation along each history path segment. Note that the counted half-cycle is associated with the minimum and maximum values of the auxiliary channel (e.g. $\sigma_{\perp min}$ and $\sigma_{\perp max}$) only between the eliminated elements, not

including the previous stack element.

After the half-cycles are counted, the associated $\sigma_{\perp min}$, $\sigma_{\perp max}$, and $\sigma_{\perp m}$ are obtained from the variation of the normal stress $\sigma_\perp$ (perpendicular to the candidate plane) along each path segment. The equivalent range $\Delta\gamma$ is then calculated for each counted half-cycle from the $\gamma_A$-$\gamma_B$ history using the MOI method or one of the convex enclosure methods presented in [4]. A shear-based model such as Fatemi-Socie's is then applied to all counted strain range $\Delta\gamma$ with the associated $\sigma_{\perp max}$ along each half-cycle to calculate the accumulated fatigue damage from Miner.

Finally, among all Case A and Case B candidate planes used in the above calculations, the one with maximum accumulated damage according to the chosen multiaxial fatigue damage model is then the critical plane where the microcrack is expected to initiate.

But it has been argued that Case B cracks suffer not only the Mode III tearing influence of $\tau_B$ at the maximum crack depth, but also the Mode II influence of the usually non-zero $\tau_A$ at the surface. The associated ranges $\Delta\tau_B$ and $\Delta\tau_A$ synergically interact, causing the crack to grow respectively in the depth and width directions under mixed Mode II-III. Under NP VAL histories, the $\tau_B$ and $\tau_A$ histories need to be counted using a two-dimensional (2D) version of the MWB multiaxial rainflow algorithm, performed on a $\tau_A \times \tau_B$ diagram. The equivalent range $\Delta\tau$ of each counted half-cycle should then be calculated from the associated 2D path segments in the $\tau_A \times \tau_B$ diagram, using a convex enclosure or the MOI methods from [4]. The accumulated Mode II-III shear damage is then obtained from Miner's rule adding the damage contributions of the equivalent $\Delta\tau/2$ and $\sigma_{\perp max}$ of each half-cycle using Findley's or McDiarmid's models. Analogously, for strain-based and energy-based criteria, for each Case B candidate plane, the $\gamma_B$ and $\gamma_A$ histories are counted using a 2D version of the MWB multiaxial rainflow algorithm, performed on a $\gamma_A \times \gamma_B$ diagram. The equivalent range $\Delta\gamma$ of each counted half-cycle is then calculated from the associated 2D path segments using a convex enclosure or the MOI methods [4], used in Fatemi-Socie's, Brown-Miller's, or Liu-II's multiaxial fatigue damage models to calculate the mixed Mode II-III damage from Miner's rule.

An alternate approach has been proposed by Carpinteri et al. in [15], where the normal stress $\sigma_\perp$ perpendicular to the crack plane is taken as the cycle counting variable, i.e. it is the main channel of a modified uniaxial rainflow algorithm. The shear components $\tau_A$ and $\tau_B$ are retained during the filtering and rainflow counting process applied to the $\sigma_\perp$ history. This method does not separate the behaviour of tensile-sensitive and shear-sensitive materials, whose damage is usually calculated respectively by SWT's and Fatemi-Socie's models. Instead, a non-linear combination of $\sigma_\perp$, $\tau_A$ and $\tau_B$ is used to define an equivalent stress amplitude and thus obtain the associated damage for each rainflow-counted event, which are combined using Miner's linear rule. Such Carpinteri-Spagnoli approach has been formulated as well in the frequency domain [16], where the determination of the critical plane orientation is obtained through the Power Spectral Density matrix of the stress tensor.

## 5. Comparison between Critical Plane and Wang-Brown Approaches

Although very general and capable of rainflow counting 6D NP histories, both the original WB and the MWB algorithms have drawbacks. In their search for individual cycles with maximum $\Delta\varepsilon_{Mises}$, they intrinsically assume that the highest fatigue damage is associated with the highest $\Delta\varepsilon_{Mises}$. This is not necessarily true, since several fatigue damage models assume a dependence on both strain amplitude and maximum or mean stresses that open or close microcracks. A path segment with a slightly lower $\Delta\varepsilon_{Mises}$ but with a much higher mean stress could cause higher fatigue damage, but it might not be identified by such algorithms, which search for load path segment combinations that maximize $\Delta\varepsilon_{Mises}$ regardless of the associated stresses. This issue would only be solved if both the stress and strain paths could be represented in a single hypothetical diagram whose metric (distance between two stress-strain states) would be proportional to the fatigue damage according to some damage model.

Another issue with rainflow counting NP multiaxial histories is whether or not to use a critical plane approach. The Wang-Brown multiaxial rainflow algorithm is general enough to be directly applied to a multiaxial history involving all six strain components. But its rainflow-counted half-cycles will probably occur on different planes, not reproducing the crack initiation mechanism from most metals.

Instead, the multiaxial VAL history could be projected onto a candidate plane, and only then should a multiaxial rainflow count be used, as performed in the critical plane rainflow approach.

This observation that some loading events may cause fatigue damage on some planes but not on others is consistent with the directional nature of fatigue damage, however it is not applicable to all materials. Critical plane models

assume that some stress or strain components may not contribute at all to the damage on the critical plane, which might not be true for certain materials, e.g. if the damage process is influenced by the hydrostatic stress. Critical plane models also implicitly assume that the crack plane does not change significantly during the early propagation of the dominant microcrack. However, despite these criticisms, the critical damage models are probably the most successful in predicting fatigue lives under multiaxial VAL [17] for materials that fail due to a single dominant crack, as in the fatigue behaviour of most metals. For such materials, the best predictions should be the ones from multiaxial models that use the critical plane idea, where the damage parameters are maximized.

## 6. Conclusions

In this work, the most commonly adopted rainflow approaches for variable amplitude non-proportional multiaxial histories have been detailed and compared. The Modified Wang Brown method is a practical tool to perform the rainflow count in 6D stress or strain histories, since the counting process only needs to be applied once for the entire 6D history. However, the resulting rainflow count might miss half-cycles that could induce significant damage on certain possible crack planes. The critical plane approach, on the other hand, requires a uniaxial or bi-dimensional rainflow counting method to be applied to every candidate plane projection of the loading history. Although computationally intensive, especially if several candidate planes are considered, the resulting rainflow-counted half-cycles better reproduce the directional nature of fatigue damage, predicting not only the accumulated damage but also the direction of the critical plane where the crack is expected to initiate. Therefore, for materials which fail due to a single dominant crack, the critical plane rainflow results in more consistent predictions than the WB or MWB methods. If, on the other hand, the material failure mechanism involves a combination of damage parameters acting on different planes, such as in certain brittle or ductile materials that fail due to a global defect caused by the coalescence of multiple microcracks or microvoids, respectively, then an invariant-based rainflow approach such as WB or MWB might be a better option to account for the contribution of all stress/strain components through the Mises metric.

## References

[1] Bannantine, JA, Socie, DF, "A variable amplitude multiaxial fatigue life prediction method," Fatigue Under Biaxial and Multiaxial Loading, ESIS Publication 10, p.35-51, 1991.
[2] Wang, CH, Brown, MW, "Life prediction techniques for variable amplitude multiaxial fatigue - part 1: theories," Journal of Engineering Materials and Technology, v.118, p.367-370, 1996.
[3] Meggiolaro, MA, Castro, JTP, "An Improved Multiaxial Rainflow Algorithm for Non-Proportional Stress or Strain Histories - Part II: The Modified Wang-Brown Method," International Journal of Fatigue, v.42, p.194-206, 2012.
[4] Meggiolaro, MA, Castro, JTP, "Prediction of non-proportionality factors of multiaxial histories using the Moment Of Inertia method," International Journal of Fatigue, v.61, pp.151-159, 2014.
[5] Sines,G "Behavior of metals under complex static and alternating stresses", in Metal Fatigue, McGraw-Hill, p.145-169, 1959.
[6] Crossland B, "Effect of large hydrostatic pressures on the torsional fatigue strength of an alloy steel," in Proceedings of International Conference on Fatigue of Metals, London: IMechE, p. 138-149, 1956.
[7] Langlais, TE, Vogel, JH, Chase, TR, "Multiaxial cycle counting for critical plane methods," International Journal of Fatigue, v.25, p.641-647, 2003.
[8] Fatemi, A, Socie, DF, "A critical plane approach to multiaxial damage including out-of-phase loading," Fatigue and Fracture of Engineering Materials and Structures v.11, p.149-166, 1988.
[9] Smith, RN, Watson, P, Topper, TH, "A stress-strain parameter for the fatigue of metals," Journal of Materials v.5(4), p.767-778, 1970.
[10] Liu, KC, "A Method Based on Virtual Strain-Energy Parameters for Multiaxial Fatigue Life Prediction," Advances in Multiaxial Fatigue, ASTM STP 1191, D.L. McDowell and R. Ellis, Eds., ASTM, p.67-84, 1993.
[11] Findley,WN "A theory for the effect of mean stress on fatigue of metals under combined torsion and axial load or bending", Journal of Engineering for Industry, p.301-306, 1959.
[12] McDiarmid, DL, "A shear stress based critical-plane criterion of multiaxial fatigue Failure for design and life prediction," Fatigue and Fracture of Engineering Materials and Structures, v.17, p.1475-1484, 1994.
[13] Brown, M, Miller, KJ, "A theory for fatigue under multiaxial stress-strain conditions", Institute of Mechanical Eng., v.187, p.745-756, 1973.
[14] McInnes, CH, Meehan, PA, "Equivalence of four-point and three-point rainflow cycle counting algorithms," International Journal of Fatigue, v.30, n.3, p.547-559, 2008.
[15] Carpinteri, A, Spagnoli, A, Vantadori, S, A multiaxial fatigue criterion for random loading. Fatigue and Fracture of Engineering Materials and Structures, v.26(6), p.515-522, 2003.
[16] Carpinteri, A, Spagnoli, A, Vantadori, S, Reformulation in the frequency domain of a critical plane-based multiaxial fatigue criterion. International Journal of Fatigue, v.67, p.55-61, 2014.
[17] Socie, DF, Marquis, GB, Multiaxial Fatigue, SAE 1999.